Editors' Suggestion

Orientation dynamics of gyrotactic microswimmers in turbulent flows

Suraj Kumar Nayak [1,*] Vishwanath Shukla [1,†] and Akshay Bhatnagar [2,‡]
[1]*Department of Physics, Indian Institute of Technology Kharagpur, West Bengal - 721 302, India*
[2]*Department of Physics, Indian Institute of Technology Roorkee, Uttarakhand - 247 667, India*

(Received 28 October 2025; accepted 6 July 2026; published 4 August 2026)

We study the dynamics of gyrotactic microswimmers suspended in homogeneous and isotropic turbulence by using direct numerical simulations. The swimmers are characterized by three nondimensional parameters: their aspect ratio (γ), a dimensionless swimming speed (ϕ), and a dimensionless reorientation time (ψ). Strong gyrotaxis (smaller ψ) promotes vertical alignment of the swimmers, while weak gyrotaxis leads to nearly isotropic orientations. At low swimming numbers, the orientation distribution is largely shape independent with spheres and spheroids showing marginally greater vertical alignment than rods, whereas at higher activity the peaks of the distributions exhibit largely shape-independent behavior and the tails show a clear dependence on particle shape. However, at large ψ rods exhibit a stronger alignment along the vertical. We observe that at small ψ the rod-shaped swimmers respond to shear by aligning with the stretching direction of the strain-rate tensor, while at large ψ the alignment with the vorticity vector is preferred. The orientation autocorrelation is found to decay exponentially, with a decay rate that scales as $1/(2\psi)$. Analysis of the mean-squared displacement reveals a transition from a ballistic motion at short times to a diffusive regime at longer times. To assess the efficiency of vertical migration, we compute the probability distributions of vertical displacement over a fixed time interval and the time taken to migrate a specific vertical distance. Furthermore, we use a simplified two-dimensional model for spherical swimmers that qualitatively reproduces the key trends observed in the full three-dimensional simulations.

DOI: 10.1103/6yn2-ckfx

I. INTRODUCTION

Marine and aquatic microorganisms often navigate through turbulent fluid flows for food, reproduction, and survival. Many of these microswimmers actively adjust their swimming behavior in response to local hydrodynamic cues, such as shear and vorticity [1–10]. An interesting class of microswimmers with asymmetrical mass distribution within their body exhibit an inherent directional bias in their motion. This directed swimming, known as gyrotaxis, arises from a subtle interplay between the viscous torque exerted by the surrounding fluid and the gravitational torque.

Experimental and numerical studies have shown that the fast-moving swimmers preferentially sample the upwelling regions of the flow, whereas the slow-moving swimmers sample the downwelling regions of the flow [1,2,5,10–15]. For example, phytoplanktons perform diel vertical migration in turbulent environments for sunlight and nutrient uptake [1,2,5,12,14,16,17]. Also, in

*Contact author: surajkumarnayak96@gmail.com
†Contact author: vishwanath.shukla@phy.iitkgp.ac.in
‡Contact author: akshayphy@gmail.com

high shear regions, the natural alignment of the microswimmers is disrupted and they undergo tumbling motion, leading to the formation of thin layers that can range from a few centimeters to meters in thickness and extend over several kilometers horizontally. These layers can occur in laminar as well as turbulent flows and hinder the sunlight penetration, increase zooplankton and fish mortality, and at times can trigger harmful algal blooms [4,13,18,19]. Also, the gyrotaxis enables these organisms to orient and migrate preferentially in the flow, often leading to striking cluster patterns in turbulent environments [4,10,11,16,20–24], which can be fractal [2,3,5,12,25]. The clustering depends on the shape; spherical swimmers show stronger clustering compared to the prolate or rodlike swimmers [2,3,5,10–13,15,25]. Moreover, their preferential transport and dispersion for foraging and survival in laminar and turbulent flows has been extensively studied [6,9,10,13,14,23,26,27]. However, the orientation statistics of these microswimmers remains relatively less explored.

Gyrotactic microswimmers have a natural tendency to align vertically as a result of their bottom heaviness [16,20,22,28]. This has been examined both experimentally and theoretically for simple flows; for example, gyrotaxis leads to the formation of bioconvection patterns, wherein particles swim upward to the top and fall as plumes with velocity greater than the flow velocity [16,20,28]. The local equilibrium orientations of these swimmers have been studied in a variety of experimental setups, such as the vertical Poiseuille flow in a pipe, conical sink flows, two-dimensional (2D) shear flows, and the wake of a falling sphere [28].

The axisymmetric rodlike microscopic tracer particles are known to exhibit strong alignment with the vorticity vector in turbulent flows and a good alignment with the strain-rate-tensor eigenvector associated with the largest eigenvalue [29]. In Refs. [30–32], the alignment of nonspherical active particles in chaotic, moderately turbulent flows was studied; the rodlike active particles were found to preferentially align with the flow velocity. Also, a comparison of gyrotactic and nongyrotactic swimmers reveals differences in how they align with the vorticity and strain-rate eigenvectors [25]. Moreover, when the swimming velocity is increased, the alignment with the Lagrangian stretching direction is reduced in the presence of a weak gyrotaxis, whereas it is enhanced if the gryotaxis is strong [15]. In Ref. [33], the solutions to the Reynolds-averaged equations for the orientation probability distribution function of spheroidal swimmers in the long-time limit were found to be a one-parameter Fisher distribution.

In this study, we carry out a systematic investigation of the orientation statistics of gyrotactic microswimmers in a turbulent flow using direct numerical simulations (DNS). We consider three different aspect ratios: spheres, spheroids, and rods. The orientation distribution is influenced by the flow gradients, swimmer geometry, and the gyrotactic response. We find that the strongly gyrotactic microswimmers predominantly align with the vertical, while weakly gyrotactic swimmers exhibit nearly isotropic orientation distribution; the alignment is more enhanced for the spheres and spheroids compared to the rods. The rod-shaped swimmers are more influenced by the shear in the flow and tend to align with the eigenvector corresponding to the largest eigenvalue of the strain-rate tensor. The rate of exponential decay of the orientation autocorrelations depends on the gyrotactic response time. All the swimmers exhibit ballistic and diffusive transport at short and long times, respectively, irrespective of their gyrotactic strength. A two-dimensional reduced model for spherical swimmers is able to capture the key features of the orientation and transport statistics.

The remainder of this paper is structured as follows. In Sec. II, we discuss the model and the numerical methods, followed by the presentation of our DNS results in Sec. III. Section IV contains a discussion of the reduced model. We give our conclusions in Sec. V.

II. MODEL AND NUMERICAL SETUP

We consider a dilute concentration of gyrotactic microswimmers in a turbulent incompressible three-dimensional (3D) fluid flow. The spatiotemporal evolution of the incompressible fluid velocity

field $\mathbf{u}(\mathbf{x}, t)$ is governed by the Navier-Stokes equations (NSEs),

$$\frac{\partial \mathbf{u}}{\partial t} + (\mathbf{u} \cdot \boldsymbol{\nabla})\mathbf{u} = -\boldsymbol{\nabla} p + \nu \nabla^2 \mathbf{u} + \mathbf{f}, \tag{1a}$$

$$\boldsymbol{\nabla} \cdot \mathbf{u} = 0, \tag{1b}$$

where $p(\mathbf{x}, t)$ is the pressure field and ν is the kinematic viscosity. We set the fluid density $\rho = 1$ without any loss of generality. The external body force $\mathbf{f}(\mathbf{x}, t)$ helps maintain a statistically stationary state by injecting energy at large length scales. The injected energy cascades down to the viscous dissipation length scales, characterized by the Kolmogorov scale, $\eta = (\nu^3/\epsilon)^{1/4}$, where ϵ is the energy dissipation rate. The timescale and the velocity associated with η are $\tau_\eta = (\nu/\epsilon)^{1/2}$ and $u_\eta = (\nu\epsilon)^{1/4}$, respectively. The turbulent flow is characterized by the Taylor-scale Reynolds number $\mathrm{Re}_\lambda = (u_{\mathrm{rms}}\lambda)/\nu$, where $u_{\mathrm{rms}} = \sqrt{\langle |\mathbf{u}|^2 \rangle/3}$ is the root-mean-squared velocity and $\lambda = \sqrt{15\nu u_{\mathrm{rms}}^2/\epsilon}$ is the Taylor microscale.

In gyrotactic microswimmers the geometric center and the center of mass do not coincide because of asymmetric mass distribution; as a result these bottom-heavy swimmers have a natural tendency to swim vertically upward. We consider gyrotactic microswimmers of size smaller than the Kolmogorov length scale, and their density is close to the fluid density. We prescribe the following equations for the dynamical evolution of the position ($\mathbf{x}$) and the orientation ($\mathbf{p}$) of the microswimmers,

$$\dot{\mathbf{x}} = \mathbf{u}(\mathbf{x}, t) + v_s \mathbf{p}, \tag{2a}$$

$$\dot{\mathbf{p}} = \frac{[\hat{\mathbf{z}} - (\hat{\mathbf{z}} \cdot \mathbf{p})\mathbf{p}]}{2B} + \frac{\boldsymbol{\omega} \times \mathbf{p}}{2} + \gamma[\mathbf{S}\mathbf{p} - (\mathbf{p} \cdot \mathbf{S}\mathbf{p})\mathbf{p}], \tag{2b}$$

where v_s is the self-propulsion speed, B is the gyrotactic reorientation time, $|\mathbf{p}| = 1$, $\hat{\mathbf{z}}$ is the unit vector along the z axis (the vertical direction), and γ is the aspect ratio of the microswimmer. $\boldsymbol{\omega} = \boldsymbol{\nabla} \times \mathbf{u}$ and $\mathbf{S} = (1/2)[\boldsymbol{\nabla}\mathbf{u} + (\boldsymbol{\nabla}\mathbf{u})^T]$ are the fluid vorticity and the symmetric part of the strain-rate tensor, respectively, at the swimmer's position.

The first term on the right-hand side of Eq. (2b) describes the reorientation of the microswimmers toward the vertical direction [21]. We define a stability number, $\psi = B/\tau_\eta$, as the ratio of the reorientation time toward the z axis to the Kolmogorov time. The second and the third terms describe the rotation due to the local vorticity and the local strain rate, respectively, experienced by the swimmers due to the flow [21]. The latter depends on the shape of the microswimmer, characterized by $\gamma = (l^2 - d^2)/(l^2 + d^2)$, where l is the length of the swimmer in the direction of $\mathbf{p}$ and d is the width. In our study, we neglect the inertia of the swimmers, the interactions among the swimmers, and the backreaction of swimmers on the flow.

We perform direct numerical simulations (DNS) of the incompressible three-dimensional (3D) NSE equations (1) using a pseudospectral method with 2/3 dealiasing rule on a triply periodic domain of length 2π. We use a second-order, exponential Adams-Bashforth scheme for time marching and a constant-energy-forcing scheme to maintain the flow in a steady state. Our DNS runs involve 256^3 collocation points; the resulting turbulent flow has $\mathrm{Re}_\lambda \approx 120$ with $k_{\max}\eta > 1.1$. We integrate Eqs. (2a) and (2b) for 10^6 swimmers by using a trilinear interpolation to compute the velocity and its gradients at the swimmer's position. We explore the orientation dynamics for a wide range of parameters: the stability number $\psi = (0.5,\ 1,\ 10)$ and the swimming number $\phi \equiv v_s/u_\eta \in [0 : 10]$ for three different aspect ratios $\gamma = 0$, 0.5, and 1 that correspond to spheres, spheroids, and rodlike swimmers, respectively. We initialize the swimmers at uniform random positions when the background turbulent flow has attained a steady state. For the convergence of statistical quantities, we perform the DNS run for several eddy turnover times. Also, to obtain a good estimate of the mean-squared displacement, we use 10^5 swimmers and integrate the equations over 50 eddy turnover times. In Table I, we present the summary of the parameters used in our DNS run.

TABLE I. Table of parameters for the DNS run with N^3 collocation points. δt is the time step, ν is the kinematic viscosity, N_p is the number of microswimmers, and ϵ is the mean rate of energy dissipation. $\eta = (\nu^3/\epsilon)^{1/4}$, $\tau_\eta = (\nu/\epsilon)^{1/2}$, and $u_\eta = (\nu\epsilon)^{1/4}$ are the Kolmogorov dissipation length scale, timescale, and velocity, respectively. $\lambda = \sqrt{15\nu u_{\rm rms}^2/\epsilon}$ is the Taylor microscale, $\mathrm{Re}_\lambda = (u_{\rm rms}\lambda)/\nu$ is the Reynolds number based on λ and $\tau_{\rm eddy} = (\sum_k \frac{E(k)/k}{E})/u_{\rm rms}$ is the large eddy turnover time, where $E(k)$ is the energy spectrum of the flow, E is the total energy, and $u_{\rm rms}$ is the root-mean-squared velocity of the flow.

N	δt	ν	N_p	$k_{\rm max}\eta$	Re_λ	ϵ	η	λ	τ_η	$\tau_{\rm eddy}$	u_η
256	5×10^{-4}	2.5×10^{-3}	10^6	1.14	120	0.5	0.01	0.29	0.07	2.19	0.19

III. RESULTS

A. Orientation dynamics

The projections of the orientation vector $\mathbf{p}$ along the x, y, and z directions are given by $p_x \equiv \mathbf{p}\cdot\hat{\mathbf{x}} = \cos\theta_1$, $p_y \equiv \mathbf{p}\cdot\hat{\mathbf{y}} = \cos\theta_2$, and $p_z \equiv \mathbf{p}\cdot\hat{\mathbf{z}} = \cos\theta_3$, respectively. In Fig. 1 we show the orientation of swimmers in the $p_x p_y p_z$ space for large and small reorientation times; a particular orientation $\mathbf{p}$ appears as a point (blue dot) on the unit sphere. For large ψ, the orientation vector $\mathbf{p}$ is likely to explore all the possible directions, but with a slightly marked tendency to point along $\hat{\mathbf{z}}$. In contrast, for the small value of ψ, swimmers are predominantly directed along $\hat{\mathbf{z}}$ and their spread over the unit sphere is significantly reduced; see Fig. 1. This can be understood by comparing the gyrotactic reorientation time with the characteristic timescale of the flow. For smaller values of the reorientation time (ψ), gyrotactic torques act more rapidly than the typical rotational fluctuations induced by the flow, leading to a more efficient alignment of the swimmers with the vertical direction ($\hat{\mathbf{z}}$). In contrast, for larger ψ, reorientation is slower and the flow-induced rotations allow the orientation vector to explore a broader range of directions, resulting in a nearly isotropic distribution with only a weak preferential alignment.

We quantify this alignment tendency by computing the probability distribution function (PDF) of $\cos\theta_3$, given that the direction of gyrotaxis is $\hat{\mathbf{z}}$. In Figs. 2(a)–2(c), we show the PDFs $P(\cos\theta_3)$ for swimming numbers $\phi = 0$, 1, and 10, respectively, for different stability numbers ψ and aspect ratios γ. The three sets of colors—orange, green, and blue—correspond to $\psi = 0.5$, 1, and 10, respectively. Moreover, the three shades of the same color, in increasing order of their lightness, correspond to three different values of γ, i.e., spheres ($\gamma = 0$, circle markers), spheroids ($\gamma = 0.5$, diamond markers), and rods ($\gamma = 1$, square markers). In the absence of activity, $\phi = 0$, the swimmers behave like tracers; see Fig. 2(a). For low stability numbers $\psi = 0.5$ (orange shaded curves) and $\psi = 1$ (green shaded curves) swimmers show a strong alignment with the $\hat{\mathbf{z}}$ direction, with peaks that are approximately 5 times stronger than that of the latter. However, the alignment probability decreases very rapidly as θ_3 increases away from zero. Furthermore, for a very large stability number $\psi = 10$, the distribution becomes nearly flat, suggesting that the swimmers are able to explore all the possible directions, but the gyrotaxis along $\hat{\mathbf{z}}$ leads to a small nonzero slope.

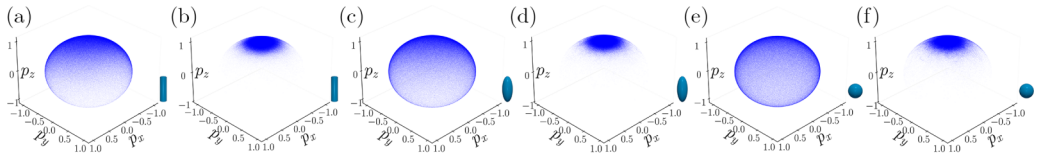

FIG. 1. Orientation distribution in $p_x p_y p_z$ space. Rodlike microswimmers for (a) $\psi = 10$ and (b) $\psi = 0.5$. Spheroids for (c) $\psi = 10$ and (d) $\psi = 0.5$. Spheres for (e) $\psi = 10$ and (f) $\psi = 0.5$. Swimming number is kept fixed at $\phi = 10$. Projections of the orientation vector along $\hat{\mathbf{x}}$, $\hat{\mathbf{y}}$, and $\hat{\mathbf{z}}$ are given by $p_x \equiv \mathbf{p}\cdot\hat{\mathbf{x}}$, $p_y \equiv \mathbf{p}\cdot\hat{\mathbf{y}}$, and $p_z \equiv \mathbf{p}\cdot\hat{\mathbf{z}}$, respectively.

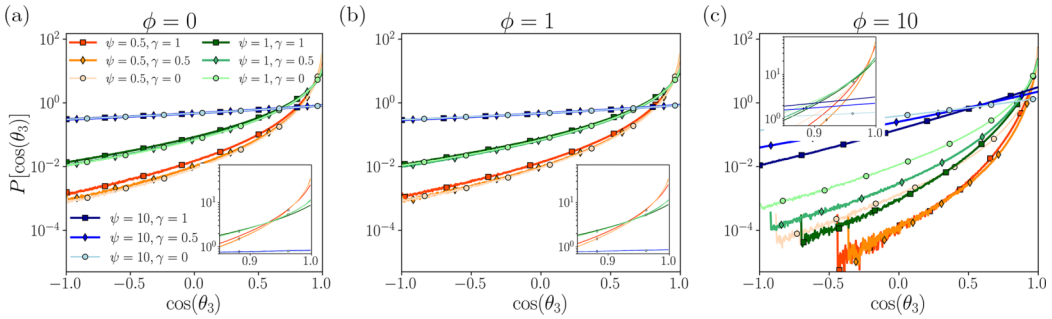

FIG. 2. Probability distribution functions of $\cos\theta_3 (\equiv \mathbf{p}\cdot\hat{\mathbf{z}})$ for swimming numbers: (a) $\phi = 0$, (b) $\phi = 1$, and (c) $\phi = 10$. Behavior is shown for the stability numbers $\psi = 0.5$ (orange curves), 1 (green curves), and 10 (blue curves). Each (ϕ, ψ) combination is explored for three shapes: rods ($\gamma = 1$, square markers), spheroids ($\gamma = 0.5$, diamond markers), and spheres ($\gamma = 0$, circle markers). The inset shows the magnified part of the peaks of the distributions in the main figure. The color and marker representations indicated in the legend of the first plot are common to all plots in the figure.

Figure 2(b) shows that the qualitative behavior of the PDFs does not change when we increase the swimming number to $\phi = 1$. Also, for these swimming numbers, we do not observe any significant dependence of orientation on the aspect ratio.

Figure 2(c) shows that the tendency to align with $\hat{\mathbf{z}}$ is enhanced for the fast swimmers ($\phi = 10$). In agreement with this, the tails of the PDFs fall more rapidly, suggesting a reduction in chances of antialignment with $\hat{\mathbf{z}}$. Also, we observe a clear dependence on the shape of the swimmers. We note that for small ψ, the peaks of the distributions indicate that spherical and spheroidal swimmers exhibit a marginally greater alignment tendency compared to rodlike swimmers, whereas an opposite trend is observed for $\psi = 10$. For the case with the largest reorientation time ($\psi = 10$), the orientation distribution is relatively flat, but the above shape dependence is clearly evident. We observe that, as ψ increases, the orientation distribution becomes broader, indicating a higher likelihood of antialignment among particles. For the same ψ, spherical swimmers show a stronger tendency toward antialignment compared to others. Since the swimmers mostly prefer to orient along the vertical direction, the PDFs of the orientation along the x and y directions are Gaussian with zero mean (data not shown).

We remark that even though the swimming number does not appear in the governing equation for the orientation $\mathbf{p}$, a considerable change in the alignment of the swimmers in the vertical direction is observed as we change ϕ. Note that the orientation dynamics is controlled by the effects of vorticity and strain rate in the flow, which in turn lead to dissimilar effects on swimmers depending on their self-propulsion speed, hence the nontrivial effect. Also, the orientation dynamics depends on the aspect ratio—the rods experience more shear from the flow than the spheres; see Fig. 2(c).

We further characterize the orientation dynamics by computing the PDFs of the cosine of the angles that $\mathbf{p}$ makes with the three normalized eigenvectors of the strain-rate tensor $(\mathbf{e}_1, \mathbf{e}_2, \mathbf{e}_3)$ and the normalized local vorticity vector $\mathbf{e}_\omega$ for $\phi = 1$; the corresponding eigenvalues of $(\mathbf{e}_1, \mathbf{e}_2, \mathbf{e}_3)$ satisfy $\lambda_1 < \lambda_2 < \lambda_3$. We recall that for $\phi = 1$, the self-propulsion speed is equal to the Kolmogorov velocity. In Figs. 3(a)–3(c), we show the PDFs of $\mathbf{p}\cdot\mathbf{e}_i$ (where $i = 1, 2, 3, \omega$) for the rodlike swimmers and the stability numbers $\psi = 0.5$, 1, and 10, respectively. We find that the swimmers are mostly oriented perpendicular to $\mathbf{e}_1$ (blue solid curves), but are parallel to $\mathbf{e}_2$ and $\mathbf{e}_3$ to a varying extent for small ψ (quick reorientation time). However, the degree of alignment or antialignment with $\mathbf{e}_\omega$ increases considerably for a large stability number $\psi = 10$ (large reorientation time). Also, we find that the PDFs of alignment with the strain-rate eigenvectors $\mathbf{e}_2$ and $\mathbf{e}_3$ are very asymmetric for $\psi = 0.5$ and 1; this asymmetry decreases as ψ increases, and the PDFs are almost symmetric for $\psi = 10$.

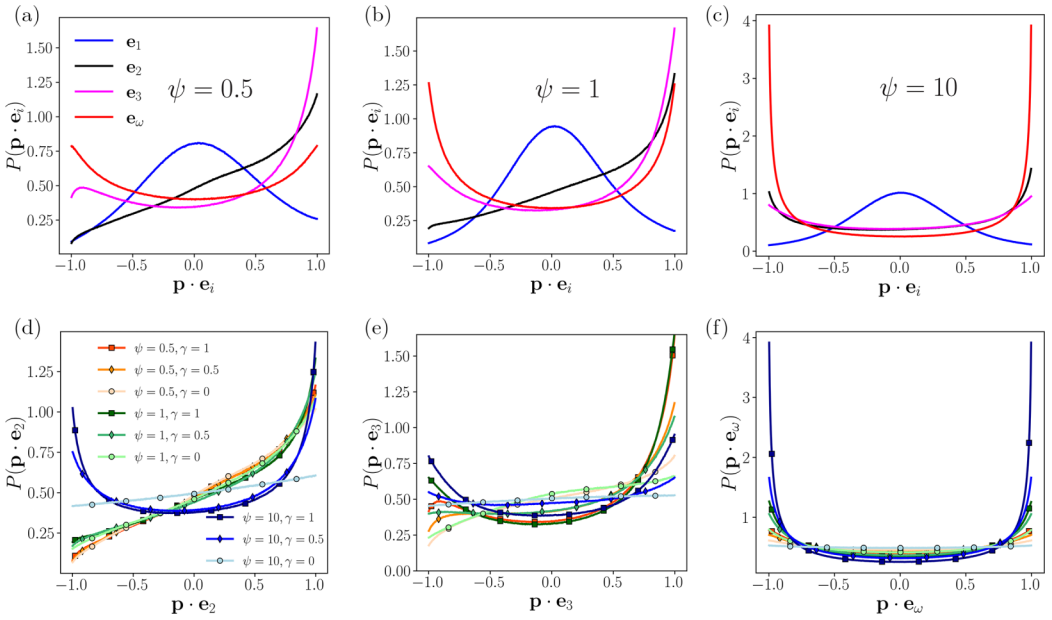

FIG. 3. Probability distribution functions (PDFs) of the projections of $\mathbf{p}$ along the normalized eigenvectors of strain-rate tensor and the normalized vorticity for $\phi = 1$ and $\gamma = 1$ with reorientation time: (a) $\psi = 0.5$, (b) $\psi = 1$, and (c) $\psi = 10$. PDFs of $\mathbf{p}\cdot\mathbf{e}_i$ for $\phi = 1$, and different values of ψ and γ, $\mathbf{e}_i$ correspond to (d) $\mathbf{e}_2$, (e) $\mathbf{e}_3$, and (f) $\mathbf{e}_\omega$. The eigenvalues of the strain-rate tensor follow the order $\lambda_3 > \lambda_2 > \lambda_1$. The plots with orange, green, and blue correspond to $\psi = 0.5$, $\psi = 1$, and $\psi = 10$, respectively. The square, diamond, and circle markers correspond to the three shapes of swimmers: rods ($\gamma = 1$), spheroids ($\gamma = 0.5$), and spheres ($\gamma = 0$), respectively. For clarity, the legend is shown only in the first plot of each row; the same color and marker conventions apply to all other plots in the corresponding row.

Next, we compare the alignment of the swimmers with the eigenvector directions of the strain-rate tensor and vorticity for different values of γ and ψ. In Figs. 3(d)–3(f) we show the PDFs of alignment of the orientation vector with $\mathbf{e}_2$, $\mathbf{e}_3$, and $\mathbf{e}_\omega$, respectively, at $\phi = 1$. Figure 3(d) suggests that swimmers, irrespective of their shape and the reorientation time, prefer to align parallel to $\mathbf{e}_2$; however, for large reorientation time, the particle shape asymmetry not only leads to a comparatively stronger alignment, but significantly enhances the chances of antialignment. Interestingly, Fig. 3(e) shows that the alignment of swimmers with $\mathbf{e}_3$ depends considerably on the shape and the reorientation time. Asymmetry and quick-to-moderate reorientation times lead to stronger parallel alignment with $\mathbf{e}_3$, whereas any decrease in asymmetry and increase in the reorientation time can significantly lower the alignment and result in broader PDFs. In fact, at large ψ the generally favored alignment of rodlike swimmers is comparatively reduced and leads to broader PDFs, which suggests a reduction in preferential alignment. Finally, Fig. 3(f) shows that larger reorientation time favors an enhanced alignment or antialignment with $\mathbf{e}_\omega$. The effect is stronger for asymmetric swimmers. For spherically symmetric swimmers the PDFs are relatively flat, suggesting an absence of preferential alignment.

In 3D turbulence, vortical structures are predominantly linelike or sheetlike. As a consequence of this geometry, the vorticity vector $\mathbf{e}_\omega$ tends to be perpendicular to the most extensional ($\mathbf{e}_3$) and most compressional ($\mathbf{e}_1$) eigenvectors of the strain-rate tensor, and exhibits a preferential alignment with the intermediate eigenvector $\mathbf{e}_2$ [34]. It therefore follows that the swimmers which align with $\mathbf{e}_2$ would also align with $\mathbf{e}_\omega$. However, we observe that swimmers with high gyrotaxis align with $\mathbf{e}_2$ and show isotropic alignment with $\mathbf{e}_\omega$ as seen in Figs. 3(d) and 3(f). Also, a shape dependence in

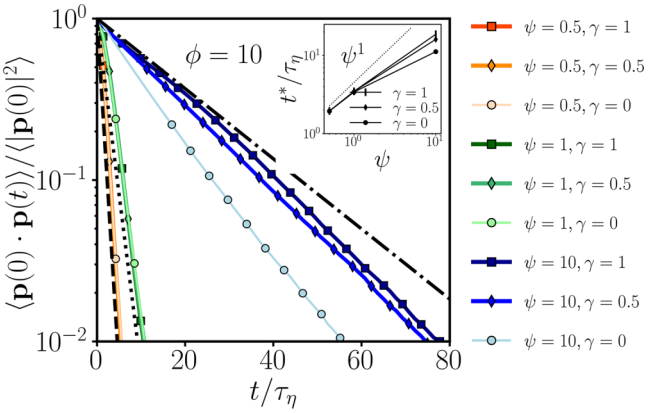

FIG. 4. Plots of orientation autocorrelation function $\mathcal{A}_\mathbf{p}(t)$ for different aspect ratios and stability numbers at swimming number $\phi = 10$. The analytically predicted decay rate $\lambda = 1/2\psi$ is indicated by dashed line ($\psi = 0.5$), dotted line ($\psi = 1$), and dot-dashed line ($\psi = 10$). Inset: Decorrelation time vs stability number ψ for rods ($\gamma = 1$), spheroids ($\gamma = 0.5$), and spheres ($\gamma = 0$). The plots with orange, green, and blue correspond to $\psi = 0.5$, $\psi = 1$, and $\psi = 10$, respectively. The square, diamond, and circle markers correspond to the three shapes of swimmers: rods ($\gamma = 1$), spheroids ($\gamma = 0.5$), and spheres ($\gamma = 0$), respectively.

the alignment statistics for low gyrotactic swimmers is observed. In particular, elongated swimmers (rods and spheroids) exhibit a tendency to both align and antialign with $\mathbf{e}_2$ and $\mathbf{e}_\omega$. This is due to the fact that the swimmers' reorientation time is long compared to the characteristic timescale of flow-induced rotation. As a result, the elongated swimmers are most affected by the flow gradients.

B. Orientation autocorrelation

We define the orientation autocorrelation as

$$\mathcal{A}_\mathbf{p} = \frac{\langle \mathbf{p}(0) \cdot \mathbf{p}(t) \rangle}{\langle |\mathbf{p}(0)|^2 \rangle}, \tag{3}$$

where $\mathbf{p}(0)$ is the orientation vector at $t = 0$. In Fig. 4 we show $\mathcal{A}_\mathbf{p}$ versus t/τ_η for different shapes and reorientation times at a fixed swimming number $\phi = 10$. The autocorrelation decays exponentially with a decay rate that depends strongly on the stability number ψ. For $\psi = 10$ the decay occurs over a long period $t \approx 75\tau_\eta$, whereas for $\psi = 0.5$ and 1 the decay period is significantly short, $t \leqslant 10$. We find that the orientation autocorrelation for fast swimmers decays as $\mathcal{A}_\mathbf{p} \propto C_0 e^{-\lambda \frac{t}{\tau_\eta}}$, with $\lambda = 1/2\psi$. We estimate the decorrelation time t^* as the interval over which $\mathcal{A}_\mathbf{p}(t^*) = \mathcal{A}_\mathbf{p}(0)/e$ and show its variation with ψ in the inset of Fig. 4 for three different shapes. We observe a deviation from linearity at large ψ, which is more pronounced for the spheres. Note that spherical swimmers with large reorientation time constitute an exception, as $\mathcal{A}_\mathbf{p}$ decays with rate, $\lambda \approx 1/\psi$. For $\phi = 0$ and 1, the autocorrelation drops to zero over relatively shorter intervals $6\tau_\eta$, $10\tau_\eta$, and $25\tau_\eta$ for $\psi = 0.5$, 1, and 10, respectively (data not shown). Clearly, swimmers with quick reorientation time decorrelate fast from their random initial alignment, indicating a quick memory loss of their past states.

We can understand the above exponential behavior by considering the time derivative of Eq. (3) and using Eq. (2b) to obtain

$$\frac{d\mathcal{A}_\mathbf{p}}{dt} = \frac{1}{\langle |\mathbf{p}(0)|^2 \rangle} \left\langle \mathbf{p}(0) \cdot \frac{[\hat{\mathbf{z}} - (\hat{\mathbf{z}} \cdot \mathbf{p})\mathbf{p}]}{2B} + \mathbf{p}(0) \cdot \frac{\boldsymbol{\omega} \times \mathbf{p}}{2} + \mathbf{p}(0) \cdot \gamma[\mathbf{Sp} - (\mathbf{p} \cdot \mathbf{Sp})\mathbf{p}] \right\rangle.$$

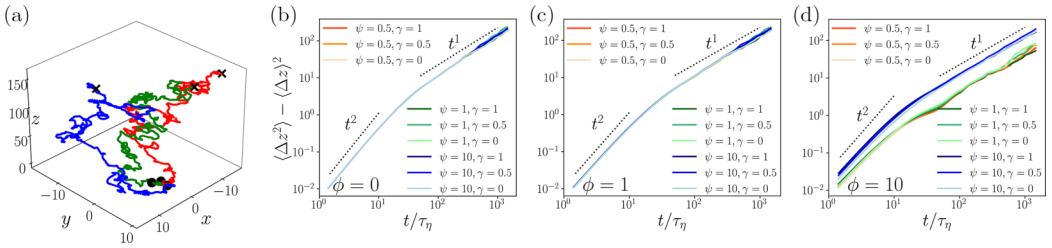

FIG. 5. (a) Trajectories of three randomly chosen swimmers, where ● and × mark the starting and ending positions, respectively. Mean-squared displacement along the vertical direction for swimming numbers: (b) $\phi = 0$, (c) $\phi = 1$, and (d) $\phi = 10$. For each ϕ, following values of $\psi = (0.5, 1, 10)$ and aspect ratios $\gamma = (1, 0.5, 0)$ were considered.

Figure 4 suggests that $\mathcal{A}_\mathbf{p}$ is almost independent of the aspect ratio for any given ψ in our DNS results. Hence, we neglect the last term in the above equation. Also, as the reorientation time is smaller than the vorticity timescale for low values of ψ, the gyrotaxis term dominates. Therefore, the second term can be neglected. The term $\langle \mathbf{p}(0) \cdot \hat{\mathbf{z}} \rangle$ averages to zero, and we make a reasonable assumption that the swimmers with low ψ are well aligned with the vertical direction, $(\hat{\mathbf{z}} \cdot \mathbf{p})$ approaches unity. These along with the definition $\psi = B/\tau_\eta$ give $d\mathcal{A}_\mathbf{p}/dt \approx -(1/2\psi\tau_\eta)\mathcal{A}_\mathbf{p}$, whose solution is $\mathcal{A}_\mathbf{p} \approx C_0 e^{-\frac{1}{2\psi}\frac{t}{\tau_\eta}}$. This suggests that the gyrotactic terms play the dominant role in the decorrelation of swimmer orientation.

C. Transport

We examine the transport of microswimmers by computing the mean-squared displacement (MSD),

$$\langle \delta \mathbf{r}^2 \rangle = \left\langle \frac{1}{N} \sum_{i=1}^{N} |\mathbf{r}_i(t) - \mathbf{r}_i(0)|^2 \right\rangle, \tag{4}$$

where $\mathbf{r}_i(0)$ is the initial position. The gyrotactic microswimmers tend to align along the vertical direction, so they spend a considerable time traveling in the vertical direction compared to the horizontal direction. Figure 5(a) shows the expected comparative extent of the trajectories along the x, y, and z directions' microswimmers are predominantly displaced along the z direction. Therefore, while accounting for this bias, we compute the MSD of the swimmers in the z direction as

$$\langle \Delta z^2 \rangle = \langle \delta z(t)^2 \rangle - \langle \delta z(t) \rangle^2, \tag{5}$$

where $\delta z = |z_i(t) - z_i(0)|$. Figures 5(b)–5(d) show the MSD $\langle \Delta z^2 \rangle$ for swimming numbers $\phi = 0$, 1, and 10, respectively. These plots unequivocally show that the swimmers, irrespective of their shape and stability numbers, exhibit a ballistic motion $\langle \Delta z^2 \rangle \propto t^2$ at short intervals and a diffusive behavior at long intervals $\langle \Delta z^2 \rangle \propto t$.

To further characterize the transport of microswimmers, we compute the distribution of vertical displacement in a given time interval. In Fig. 6(a), we show PDFs for the fixed time interval $1.4\tau_\eta$ and $\phi = 10$. We find that the distributions, in general, are asymmetric. For small stability numbers (fast reorientation times), for example, $\psi = 0.5$ and 1, the observed distributions are narrow with a larger net positive displacement; the PDFs peak at $\Delta z = 20\eta$. However, the left tail of the PDF significantly broadens as ψ is increased to 10, now covering nearly equal ranges of positive and negative displacements. Also, the dependence on the aspect ratio is either relatively weak or altogether absent. Moreover, for reduced swimming numbers, both the extent of the distribution as well as the mean displacement are reduced. In Fig. 6(b), we show the distribution of the time taken to cover a fixed vertical distance 1000η for $\phi = 10$. The tails of the PDFs $P(t/\tau_\eta)$ exhibit power

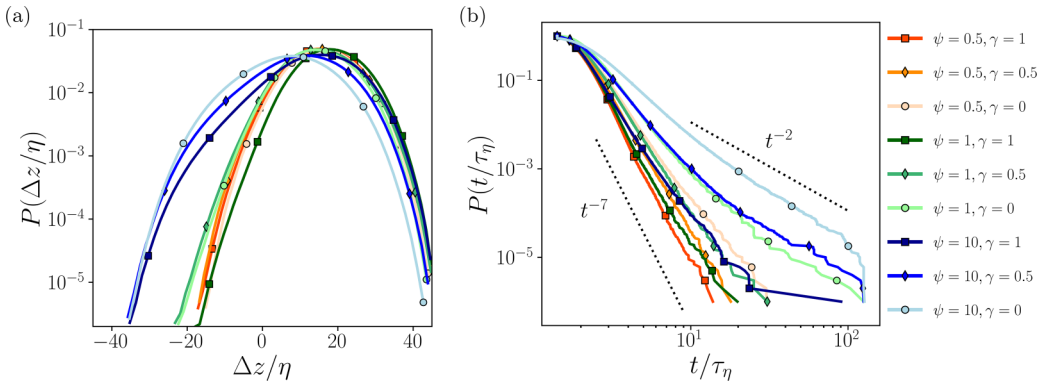

FIG. 6. Probability distribution functions of (a) the vertical displacement Δz in a fixed time interval of $1.4\tau_\eta$ and (b) the time taken to cover a fixed vertical displacement of 1000η. The swimming number $\phi = 10$ is held fixed, while the combinations of $\psi = (0.5, 1, 10)$ and $\gamma = (1, 0.5, 0)$ were considered. The plots with orange, green, and blue correspond to $\psi = 0.5$, $\psi = 1$, and $\psi = 10$, respectively. The square, diamond, and circle markers correspond to the three shapes of swimmers: rods ($\gamma = 1$), spheroids ($\gamma = 0.5$), and spheres ($\gamma = 0$), respectively.

laws $t^{-\beta}$, with exponents that strongly depend on the aspect ratio. As ψ decreases, the exponent β increases from 2 to 7. Also, for a given ψ, the exponents order as $\beta_{\text{rods}} > \beta_{\text{spheroids}} > \beta_{\text{sphere}}$. This is consistent with the findings of [35], which show that chain formation can enhance the vertical migration rate of phytoplankton.

IV. REDUCED MODEL

We use a reduced model to capture essential features of the orientation dynamics obtained using the DNS run. It qualitatively interprets the DNS results using a minimal stochastic model, where the turbulent velocity field is represented by Gaussian random noise, capturing the essential trends without the complexity of fully resolved turbulence. For simplicity, we consider a 2D model and focus only on spherical microswimmers $\gamma = 0$, wherein gyrotaxis occurs along the z axis [19,36]. We replace the background flow velocity $\mathbf{u}(\mathbf{x}, t)$ in Eq. (2a) and the vorticity in Eq. (2b) by Gaussian random noise $\xi \equiv (\xi_x, \xi_z)$ and ξ_θ, respectively. We prescribe $\langle \xi_i(t) \rangle = 0$ and $\langle \xi_i(t)\xi_j(t') \rangle = \sigma_i^2 \delta_{ij} \delta(t - t')$, where σ_i is the strength of the noise. Equations describing the evolution of the position and the orientation vector $\mathbf{p} \equiv (\cos\theta, \sin\theta)$ are given by

$$\dot{x} = v_s \cos\theta + \xi_x, \tag{6a}$$

$$\dot{z} = v_s \sin\theta + \xi_z, \tag{6b}$$

$$\dot{\theta} = \frac{\cos\theta}{2B} + \frac{1}{2}\xi_\theta. \tag{6c}$$

We define the swimming number as $\phi = v_s/u_{x\theta}$ and the stability number as $\psi = B\sigma_\theta^2$, where $u_{x\theta} = \sigma_x \sigma_\theta$ and $u_{z\theta} = \sigma_z \sigma_\theta$.

We perform numerical simulations of the above equations for several values of swimming and stability numbers to explore the statistics of orientation dynamics. In Fig. 7(a) we show the PDFs of orientation of swimmers along the z direction, i.e., $P(\cos\theta_2)$ for different values of ψ at fixed $\phi = 10$. We observe that the general features are similar to those observed in the DNS run. For quick reorientation time almost all the particles are oriented along the z direction. However, as we increase the reorientation time (larger ψ), the swimmers begin to explore directions away from the z axis; the tails of the PDFs become broader and fatter. A similar trend is observed for other values of the swimming number (data not shown). In Fig. 7(b), we show the orientation autocorrelation

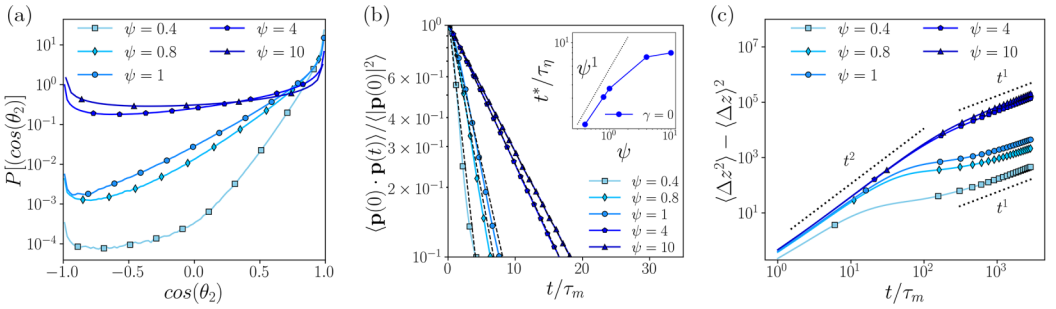

FIG. 7. Reduced model for spherical microswimmers. (a) Probability distribution of orientation about the z axis $P(\cos\theta_2)$ (b) orientation autocorrelation, and (c) mean-squared displacement along the z axis for the stability numbers $\psi = (0.4, 0.8, 2, 4, 10)$, while the swimming number is held fixed at $\phi = 10$.

functions for different values of ψ. Once again, in agreement with the DNS results, we find that $\mathcal{A}_\mathbf{p}$ decays exponentially with time and the decay rates are given by $\lambda_{\text{model}} \approx 1/2\psi$. The inset shows the linear dependence of decorrelation time with reorientation time with a small deviation at larger ψ, similar to the DNS results. Figure 7(c) shows that the MSD displays a ballistic transport at short time intervals and a diffusive behavior at large time intervals, which is in agreement with DNS results. However, we notice that the timescale associated with the crossover from the ballistic to diffusive regime increases with ψ.

In Fig. 8(a) we show the PDFs of displacement along the z direction in a fixed interval of time $1.4\tau_m$, where $\tau_m = 1/\sigma_\theta^2$. We find that the PDFs are qualitatively similar to those obtained from the DNS run. For small values of ψ, the PDFs are narrow and only positive displacements are observed. However, when ψ is increased, the PDFs become asymmetric and the left tail becomes broad. Figure 8(b) shows the PDFs of time taken to cover a fixed vertical displacement $1000\eta_m$, where $\eta_m = \sigma_x/\sigma_\theta$. The behavior is qualitatively similar to what we observe in DNSs; as we increase ψ the PDFs fall less rapidly and become fatter.

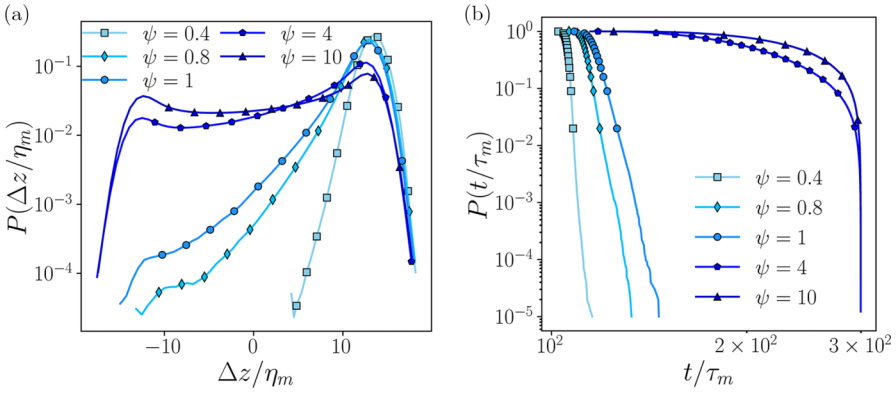

FIG. 8. Reduced model for spherical microswimmers. Probability distribution functions of (a) the vertical displacement Δz in a fixed time interval of $1.4\tau_m$ and (b) the time taken to cover a fixed vertical displacement of $1000\eta_m$ for the stability numbers $\psi = (0.4, 0.8, 2, 4, 10)$, while the swimming number is held fixed at $\phi = 10$. $\tau_m = 1/\sigma_\theta^2$ and $\eta_m = \sigma_x/\sigma_\theta$, where σ_x and σ_θ are the standard deviations of translational and rotational noise, respectively.

V. CONCLUSIONS

We examined the orientation statistics of spherical, spheroidal, and rodlike gyrotactic microswimmers in a turbulent flow. The probability distribution of the vertical alignment of swimmers exhibits a clear dependence on the gyrotaxis strength. The swimmers with higher gyrotactic strength tend to align more along the vertical direction compared to those with lower gyrotactic strength. Also, for low swimming numbers ($\phi \leqslant 1$), the orientation distribution is nearly independent of the aspect ratio (γ) considered. However, for large swimming numbers ($\phi = 10$), spheres and spheroids show marginally greater alignment with the vertical compared to rods at low ψ, but the distribution is nearly flat for high ψ with rodlike swimmers showing marginally higher alignment with the vertical.

To further understand this behavior, we examined the alignment with the strain-rate-tensor eigenvectors and the vorticity vector. Our results show that rodlike swimmers with high gyrotactic strength preferentially align with the eigenvector corresponding to the largest strain-rate eigenvalue (also known as the Lagrangian stretching direction), while those with low gyrotactic strength align more with the vorticity vector. This contrasts with the behavior of nongyrotactic swimmers, where rods tend to align more with vorticity than with strain-rate eigenvectors [25,29]. Here, we systematically compared the influence of three aspect ratios under identical turbulent and gyrotactic conditions, revealing how geometry and gyrotaxis jointly govern the alignment. We note that our results are for a modest value of $\mathrm{Re}_\lambda \approx 120$. However, the Reynolds number, along with $\gamma \in [-1, 1]$, can influence the angle between the swimming direction and the flow velocity $\cos(\theta_u) \propto \gamma \mathrm{Re}_\lambda^{-1/2}$ [31]. Similarly, preferential sampling in the vertical direction depends on both Re_λ and ψ [12]. While higher Reynolds numbers at fixed ψ enhance sampling in downwelling regions, increasing ψ reduces this tendency, causing swimmers to sample upwelling regions more frequently.

Our numerical results, along with analytical estimates, show that the orientation autocorrelation decays exponentially with rate $1/2\psi$ at high activity, mostly irrespective of the shape. However, we observe a deviation from this for spherical swimmers at large ψ. For axisymmetric nongyrotactic tracers, the decorrelation time is known to exhibit a slight increase with Reynolds number [29]. Also, we find that irrespective of their shape, gyrotactic response, and swimming number, swimmers exhibit a ballistic and a diffusive transport behavior in the short- and long-time limit, respectively. Moreover, the PDFs of time taken to cover a specified displacement exhibit power-law tails, whose exponents may depend on the gyrotactic response and the shape of microswimmers. A two-dimensional minimal model, wherein the flow velocity and its gradients are replaced by the Gaussian white noise, is able to capture the essential features of the orientation dynamics observed in the DNS run.

The present results have important implications for the ecology of motile microorganisms in natural aquatic environments. The alignment of elongated swimmers influences light penetration and scattering in the ocean, thereby affecting photosynthesis [37]. In addition, vertical migration plays a key role in regulating access to light and nutrients for phytoplankton and other microswimmers [2,34]. Our results indicate that elongated swimmers exhibit enhanced vertical migration, consistent with [35], which shows that chain formation can increase migration rates. In regions of high shear, rodlike swimmers are more susceptible to reorientation, leading to increased patchiness and the formation of thin phytoplankton layers. Such structuring can strongly influence collective behavior, promoting processes such as reproduction and competition, while also impacting light penetration; in the case of toxic blooms, it may even contribute to zooplankton and fish mortality [19].

ACKNOWLEDGMENTS

The authors acknowledge National Supercomputing Mission (NSM) for providing the computing resources of “PARAM Shakti” at IIT Kharagpur and “PARAM Porul” at NIT Trichy, which is implemented by C-DAC and supported by the Ministry of Electronics and Information Technology

(MeitY) and Department of Science and Technology (DST), along with the NSM Grant No. DST/NSM/R&D HPC Applications/2021/03.21. V.S. would like to acknowledge support from the Institute Scheme for Innovative Research and Development (ISIRD), IIT Kharagpur, Grant No. IIT/SRIC/ISIRD/2021-2022/03. S.K.N. expresses thanks for the support of the Prime Minister's Research Fellows (PMRF) scheme, Ministry of Education, Government of India.

DATA AVAILABILITY

The data that support the findings of this article are not publicly available upon publication because it is not technically feasible and/or the cost of preparing, depositing, and hosting the data would be prohibitive within the terms of this research project. The data are available from the authors upon reasonable request.

[1] W. Lampert, The adaptive significance of diel vertical migration of zooplankton, Funct. Ecol. **3**, 21 (1989).
[2] W. M. Durham, E. Climent, M. Barry, F. De Lillo, G. Boffetta, M. Cencini, and R. Stocker, Turbulence drives microscale patches of motile phytoplankton, Nat. Commun. **4**, 2148 (2013).
[3] F. De Lillo, M. Cencini, W. M. Durham, M. Barry, R. Stocker, E. Climent, and G. Boffetta, Turbulent fluid acceleration generates clusters of gyrotactic microorganisms, Phys. Rev. Lett. **112**, 044502 (2014).
[4] R. Rusconi and R. Stocker, Microbes in flow, Curr. Opin. Microbiol. **25**, 1 (2015).
[5] K. Gustavsson, F. Berglund, P. R. Jonsson, and B. Mehlig, Preferential sampling and small-scale clustering of gyrotactic microswimmers in turbulence, Phys. Rev. Lett. **116**, 108104 (2016).
[6] A. Sengupta, F. Carrara, and R. Stocker, Phytoplankton can actively diversify their migration strategy in response to turbulent cues, Nature (London) **543**, 555 (2017).
[7] A. Gupta, A. Roy, A. Saha, and S. S. Ray, Flocking of active particles in a turbulent flow, Phys. Rev. Fluids **5**, 052601(R) (2020).
[8] J. K. Alageshan, A. K. Verma, J. Bec, and R. Pandit, Machine learning strategies for path-planning microswimmers in turbulent flows, Phys. Rev. E **101**, 043110 (2020).
[9] X. Si and L. Fang, Preferential transport of swimmers in heterogeneous two-dimensional turbulent flow, Phys. Rev. Fluids **7**, 094501 (2022).
[10] J. Qiu, C. Marchioli, and L. Zhao, A review on gyrotactic swimmers in turbulent flows, Acta Mech. Sin. **38**, 722323 (2022).
[11] W. M. Durham, E. Climent, and R. Stocker, Gyrotaxis in a steady vortical flow, Phys. Rev. Lett. **106**, 238102 (2011).
[12] M. Borgnino, G. Boffetta, F. De Lillo, and M. Cencini, Gyrotactic swimmers in turbulence: Shape effects and role of the large-scale flow, J. Fluid Mech. **856**, R1 (2018).
[13] M. Cencini, G. Boffetta, M. Borgnino, and F. De Lillo, Gyrotactic phytoplankton in laminar and turbulent flows: A dynamical systems approach, Eur. Phys. J. E **42**, 31 (2019).
[14] J. D. Wheeler, E. Secchi, R. Rusconi, and R. Stocker, Not just going with the flow: The effects of fluid flow on bacteria and plankton, Annu. Rev. Cell Dev. Biol. **35**, 213 (2019).
[15] Z. Liu, L. Jiang, and C. Sun, Accumulation and alignment of elongated gyrotactic swimmers in turbulence, Phys. Fluids **34**, 033303 (2022).
[16] J. O. Kessler, Hydrodynamic focusing of motile algal cells, Nature (London) **313**, 218 (1985).
[17] D. Kamykowski, E. Milligan, and R. Reed, Relationships between geotaxis/phototaxis and diel vertical migration in autotrophic dinoflagellates, J. Plankton Res. **20**, 1781 (1998).
[18] W. M. Durham, J. O. Kessler, and R. Stocker, Disruption of vertical motility by shear triggers formation of thin phytoplankton layers, Science **323**, 1067 (2009).
[19] F. Santamaria, F. De Lillo, M. Cencini, and G. Boffetta, Gyrotactic trapping in laminar and turbulent Kolmogorov flow, Phys. Fluids **26**, 111901 (2014).

[20] J. O. Kessler, Gyrotactic buoyant convection and spontaneous pattern formation in algal cell cultures, in *Nonequilibrium Cooperative Phenomena in Physics and Related Fields* (Springer, Berlin, 1984), pp. 241–248.
[21] G. B. Jeffery, The motion of ellipsoidal particles immersed in a viscous fluid, Proc. R. Soc. London, Ser. A **102**, 161 (1922).
[22] A. Roberts, Geotaxis in motile micro-organisms, J. Exp. Biol. **53**, 687 (1970).
[23] J. G. Mitchell, A. Okubo, and J. A. Fuhrman, Gyrotaxis as a new mechanism for generating spatial heterogeneity and migration in microplankton, Limnol. Oceanogr. **35**, 123 (1990).
[24] J. S. Guasto, R. Rusconi, and R. Stocker, Fluid mechanics of planktonic microorganisms, Annu. Rev. Fluid Mech. **44**, 373 (2012).
[25] C. Zhan, G. Sardina, E. Lushi, and L. Brandt, Accumulation of motile elongated micro-organisms in turbulence, J. Fluid Mech. **739**, 22 (2014).
[26] J. R. Taylor and R. Stocker, Trade-offs of chemotactic foraging in turbulent water, Science **338**, 675 (2012).
[27] O. A. Croze, G. Sardina, M. Ahmed, M. A. Bees, and L. Brandt, Dispersion of swimming algae in laminar and turbulent channel flows: Consequences for photobioreactors, J. R. Soc. Interface **10**, 20121041 (2013).
[28] T. J. Pedley and J. Kessler, The orientation of spheroidal microorganisms swimming in a flow field, Proc. R. Soc. London, Ser. B **231**, 47 (1987).
[29] A. Pumir and M. Wilkinson, Orientation statistics of small particles in turbulence, New J. Phys. **13**, 093030 (2011).
[30] N. Pujara, M. Koehl, and E. Variano, Rotations and accumulation of ellipsoidal microswimmers in isotropic turbulence, J. Fluid Mech. **838**, 356 (2018).
[31] M. Borgnino, K. Gustavsson, F. De Lillo, G. Boffetta, M. Cencini, and B. Mehlig, Alignment of nonspherical active particles in chaotic flows, Phys. Rev. Lett. **123**, 138003 (2019).
[32] N. Pujara, J.-A. Arguedas-Leiva, C. C. Lalescu, B. Bramas, and M. Wilczek, Shape-and scale-dependent coupling between spheroids and velocity gradients in turbulence, J. Fluid Mech. **922**, R6 (2021).
[33] D. Lewis, The orientation of gyrotactic spheroidal micro-organisms in a homogeneous isotropic turbulent flow, Proc. R. Soc. London, Ser. A **459**, 1293 (2003).
[34] P. E. Hamlington, J. Schumacher, and W. J. Dahm, Direct assessment of vorticity alignment with local and nonlocal strain rates in turbulent flows, Phys. Fluids **20**, 111703 (2008).
[35] S. Lovecchio, E. Climent, R. Stocker, and W. M. Durham, Chain formation can enhance the vertical migration of phytoplankton through turbulence, Sci. Adv. **5**, eaaw7879 (2019).
[36] I. Fouxon and A. Leshansky, Phytoplankton's motion in turbulent ocean, Phys. Rev. E **92**, 013017 (2015).
[37] Marcos, J. R. Seymour, M. Luhar, W. M. Durham, J. G. Mitchell, A. Macke, and R. Stocker, Microbial alignment in flow changes ocean light climate, Proc. Natl. Acad. Sci. USA **108**, 3860 (2011).